# Characterization of Silica-Supported $Ni^{I}-H_2$ Complexes by Electron Paramagnetic Resonance and Their Titration Using CO Adsorption Measurements

**Jean-Yves Carriat, Christine Lepetit,* Maggy Kermarec, and Michel Che†**

*Laboratoire de Réactivité de Surface, UMR 7609 CNRS, Université P. et M. Curie, Tour 54-55, 2ème étage, 4, Place Jussieu, 75252 Paris Cedex 05, France*

*Received: September 30, 1997; In Final Form: January 28, 1998*

The $Ni^{I}$ species generated by UV-irradiation in the presence of hydrogen at 77 K of $Ni/SiO_2$ samples where nickel was deposited on silica using four different methods are studied by electron paramagnetic resonance. Four different signals are observed and tentatively assigned to silica-supported $Ni^{I}(H_2)_n$ complexes resulting from the reduction of two different three-coordinated $Ni^{II}$ precursors ($Ni^{II}_{3c}$). The total amount of $Ni^{I}$ obtained by photoreduction was measured using a new titration method based on CO chemisorption. The principles of this method are described. The reduction degree is related to the amount of $Ni^{II}_{3c}$ precursors. The highest reduction degree ($[Ni^{I}/Ni_{total}] = 40\%$) is obtained for samples where $Ni^{2+}$ was introduced by cationic exchange of the silica support with $[Ni(en)_3]^{2+}$ (en = ethylenediamine). The results are consistent with concomitant electron paramagnetic resonance measurements.

## Introduction

Silica-supported $Ni^{I}$ complexes have been prepared and were suggested to be active for olefin dimerization.[1] In these catalysts, $Ni^{I}$ may be obtained by irradiation of silica-supported $Ni^{II}$ precursors at 77 K in the ultraviolet (UV) range and in the presence of hydrogen.[2] This method is attractive as compared with thermal reduction as it yields selectively $Ni^{I}$, the formation of metallic nickel particles being prevented. The photoreduction method yields a mixture of silica-supported $Ni^{I}-$dihydrogen complexes as shown by electronic paramagnetic resonance (EPR).

In the past 10 years, many dihydrogen complexes of transition metals have been described, especially ruthenium or iridium ones.[3] The coordination of dihydrogen may be described similarly to the one of ethylene as explained by the *Dewar−Chatt* model.[4] This involves donation of the H−H $\sigma$ electrons into an empty $d_\sigma$ orbital of the metallic center accompanied by back-donation from a filled metal $d_\pi$ orbital into the antibonding $\sigma^*$(H−H). However, as compared to ethylene, H−H is only a single bond and if the back-bonding becomes too important, the scission of the H−H bond can occur yielding hydride complexes. More generally, depending on the efficiency of the two bonding processes, several types of complexes are observed. If both bonding types are nonefficient, unstretched dihydrogen complexes such as the Kubas complex $W(CO)_3(P^iPr_3)_2(H_2)$[5] are observed, in which the dihydrogen molecule is weakly bound and its chemical properties are very little affected. A dominant back-bonding $M(d_\pi) \rightarrow \sigma^*(H_2)$ results in a stretched unreactive coordinated dihydrogen (H−H bond length longer than 1 Å). At the opposite, a strong $H_2(\sigma) \rightarrow M(d_\sigma)$ component leads to electrophilic complexes in which the bound $H_2$ molecule exhibits an acidic character.

In this work, using various sample preparation methods, we will tentatively assign the EPR signals obtained after photoreduction under hydrogen at 77 K to different $Ni^{I}-$dihydrogen complexes and we will try to include the latter in one of the above-described classes of dihydrogen complexes.

The amount of $Ni^{I}$ obtained by photoreduction is difficult to evaluate using EPR[6,7] because there is no suitable standard. $Cu^{2+}$ complexes have often been used[8,9] but the line width and **g** tensor values of the copper−based standard are very different from the ones of the analyzed monovalent nickel complexes. The EPR titration results therefore in about 20% error. A new $Ni^{I}$ titration method, based on CO adsorption, was therefore developed in our laboratory and will be described herafter.

Recent EXAFS and diffuse reflectance studies (DRS) showed that the nickel deposition method onto the silica support strongly influences the nature of the $Ni^{II}$ precursors obtained after the thermal treatment.[10,11] The four following Ni deposition methods were investigated: (i) impregnation with $Ni(en)_3(NO_3)_2$ (samples referred to as I-Nien where en stands for ethylenediamine), (ii) cationic exchange with $[Ni(en)_3]^{2+}$ (samples referred to as E-Nien), (iii) cationic exchange with $[Ni(NH_3)]_6^{2+}$ (samples referred to as E-$NiNH_3$), and (iv) deposition−precipitation (samples referred to as DPU). The latter two methods yield a phyllosilicate[12] which decomposes during the thermal treatment into isolated three-coordinated $Ni^{2+}$ cations ($Ni^{II}_{3c}$) and in small NiO particles where nickel is six-coordinated ($Ni^{II}_{6c}$). When the first two methods are used, the presence of the chelating ligand ethylenediamine inhibits the formation of phyllosilicate; isolated $Ni^{II}_{3c}$ complexes are mainly obtained after a suitable thermal treatment together with dispersed NiO.[10] EXAFS measurements performed with the unreduced but thermally treated samples allowed selection of the cationic exchange with $[Ni(en)_3]^{2+}$ as the best route to produce isolated three-coordinated $Ni^{2+}_{3c}$ only.[11]

The nickel deposition method is expected to influence the amount of $Ni^{I}$ obtained by photoreduction of the above samples, as the latter is expected to selectively reduce the isolated three-coordinated $Ni^{2+}$ ions.[2] The aim of this work is therefore to

† Dedicated to Professor John Meurig Thomas on the occasion of his 65th birthday.

* Corresponding author. Current address: Laboratoire de Chimie de Coordination, UPR 8241 CNRS, 205 Route de Narbonne, 31077 Toulouse, France. E-mail: lepetit@lcc-toulouse.fr.

† Institut Universitaire de France.

S1089-5647(97)03189-1 CCC: $15.00 
Published on Web 04/22/1998

determine the nickel deposition method that yields the highest $Ni^I$ amount (which thus might lead to the best catalytic activity in olefin dimerization) after photoreduction. The reduction degree will be therefore measured for catalysts with similar low Ni loading (1.4%) where nickel was introduced using the four deposition methods mentioned above. After photoreduction at low temperature of the samples, the $Ni^I$ amount will be measured using CO adsorption and the results will be compared to corresponding EPR measurements.

## Experimental Section

**Samples.** *Ni Deposition Method.* Ni was deposited on Spherosil XOA 400 silica (specific surface area 400 $m^2/g$, mean pore diameter 8 nm supplied by Rhône-Poulenc) as described hereafter:

(i) Incipient wetness impregnation of $Ni(en)_3(NO_3)_2$ was performed according to the method described by Cheng et al.[13] and yielded two samples of 1.6 and 5.3 wt % nickel loading, referred to as I-Nien-1.6 and I-Nien-5, respectively.

(ii) The procedure for cationic exchange with $[Ni(en)_3]^{2+}$ was already reported by Bonneviot et al.[14] A sample E-Nien of 1.5 wt % Ni loading was obtained.

(iii) By catonic exchange with $Ni(NH_3)_6^{2+}$,[15] a sample E-$NiNH_3$ of 1.4 wt % Ni loading was prepared.

(iv) The lowest nickel loading obtained using the deposition−precipitation method with urea[16] was 2.8 wt %. The corresponding sample is referred to as DPU.

*Thermal Treatment.* The E-$NiNH_3$ samples were treated according to a procedure previously reported.[2] The latter was adjusted (oxygen flow rate, heating rate) for the other classes of samples;[10] typically, the samples were heated in flowing oxygen up to 500 °C (100 °C/h), then outgassed ($10^{-5}$ Torr) at 700 °C overnight. For I-Nien and E-Nien, the heating rate was lowered down to 50 °C/h, and the samples were maintained overnight at 500 °C under flowing oxygen before subsequent evacuation ($10^{-5}$ Torr) at 700 °C. For the DPU samples, the flowing oxygen treatment was stopped at 430 °C in order to avoid the formation of NiO, and the samples were then outgassed ($10^{-5}$ Torr) up to 700 °C.

*Photoreduction.* The photoreduction was carried out at 77 K, in a 4 mm outside diameter quartz EPR tube under 300 Torr of hydrogen or deuterium. The UV-irradiation was produced by a helical high-pressure mercury lamp with a spectral range of 250−600 nm.

*Gases.* CO and $H_2$ (Air Liquide) of high purity (>99.995%) were dehydrated over activated molecular sieves prior to use. Traces of oxygen were removed from hydrogen using an oxysorb cartridge (Air liquide).

$D_2$ (Airgaz) of high purity (>99.99995%) was used without further purification.

**Techniques.** EPR spectra were recorded at 77 K in the X-band on a Bruker ESP300E spectrometer. The amount of EPR active $Ni^I$ was determined by numerical double integration of the signals within a fixed magnetic field range (1000−5000 G) and after polynomial baseline correction. The integral intensities were normalized (corrected from the receiver gain).

CO adsorption measurements were performed using the volumetric method, at constant temperature (generally 30 °C), on 50−100 mg samples. The pressures were measured with a Datametrics 600A gauge. The volumes were determined by helium expansion in a standard volume. The isothermal CO adsorption at 7 Torr and 30 °C was complete after about 3 h.

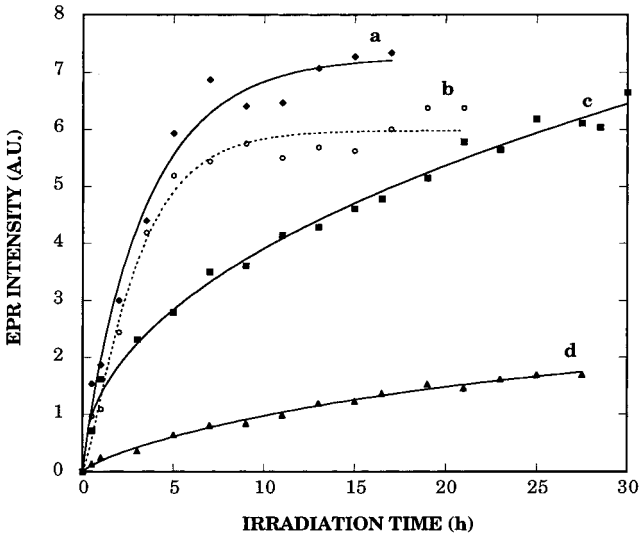


**Figure 1.** Evolution of the total EPR signal (X band, 77 K) intensity (normalized with respect to nickel content) versus UV-irradiation time at 77 K for (a) E-Nien, (b) I-Nien-1.6, (c) DPU, (d) I-Nien-5. Note that the relative EPR intensities for different samples are not comparable as the measurements were done in different EPR tubes.

## Results and Discussion

**EPR Study of the Photoreduction.** *Kinetic Considerations.* The intensity of the EPR signals was followed versus UV-irradiation time at 77 K. The EPR intensity reaches a plateau after about 10−15 h of irradiation in the case of E-Nien and I-Nien-1.6 samples with low nickel loading (Figure 1a,b), whereas the EPR intensity for the other samples (DPU and I-Nien-5) increases slowly until 25−30 h of phoreduction (Figure 1c,d). The same latter behavior was previously observed for E-$NiNH_3$.[2]

These findings suggest that two precursors may be involved in the photoreduction: the reduction of the first one **(1)** being a fast process whereas the reduction of the second one **(2)** proceeds rather slowly. A similar behavior was reported for silica−molybdena catalysts in which isolated four-coordinated $Mo^{6+}$ cations were suggested to be easily photoreduced by contrast to the slowly photoreduced polymolybdate phase.[17] The higher the coordination of the precursor or the more bulky the precursor environment, the slower the photoreduction is expected to proceed.

*EPR Signals.* After photoreduction in $H_2$, the EPR signals are broad, suggesting that there is a distribution of surface $Ni^I$ sites. When the photoreduction is carried out in $D_2$, the same EPR signals as in the presence of $H_2$ are observed, suggesting that there is no broadening due to unresolved superhyperfine structure, thus confirming the heterogeneity of the surface sites.

After 15 h of photoassisted reduction or more in $H_2$, the shape of the EPR spectrum is similar for each class of samples. By varying the experimental and EPR recording conditions, three overlapping signals were identified in the complex EPR spectrum (Figure 2). Signal **I** has an orthorhombic **g** tensor ($g_1 = 2.680$, $g_2 = 2.320$, and $g_3 = 2.003$) and was already observed during the photoreduction of E-$NiNH_3$ samples.[2] Signal **II** ($g_1 = 2.270$, $g_2 = 2.171$, and $g_3 = 2.144$) (Figure 2) and signal **III** ($g_1 = 2.366$, $g_2 = 2.215$, and $g_3 = 2.062$) exhibit the same orthorhombic symmetry.

The intensity of signal **II** increases with respect to signal **I** as the photoreduction proceeds. Indeed, signal **II** is the only one to increase after 13 h of photoreduction of E-Nien as it appears from spectra subtraction (Figure 3). The latter figure

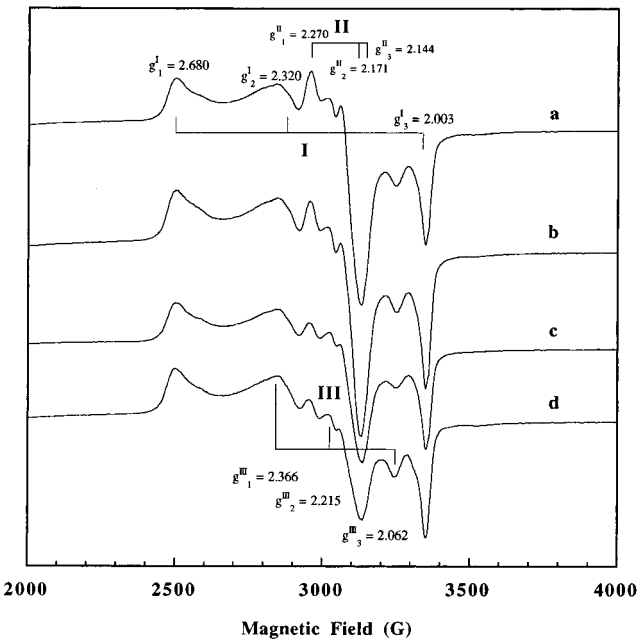


**Figure 2.** EPR spectrum (X band, 77 K) after UV-irradiation at 77 K under 300 Torr of hydrogen of (a) E-Nien during 17 h, (b) I-Nien-1.6 during 21 h, (c) DPU during 34 h, (d) E-$NiNH_3$ during 22 h.

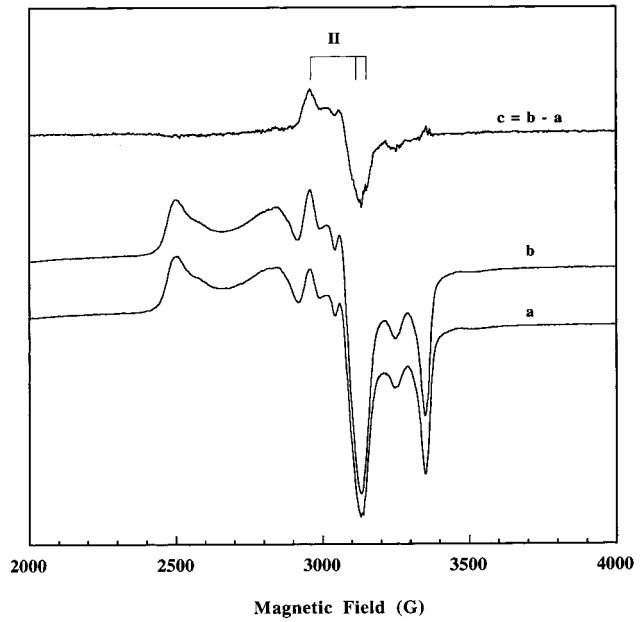


**Figure 3.** EPR spectrum (X band, 77 K) after UV-irradiation at 77 K under 300 Torr of hydrogen of E-Nien-1.5 (a) during 7 h, (b) during 17 h, (c) spectra difference b − a.

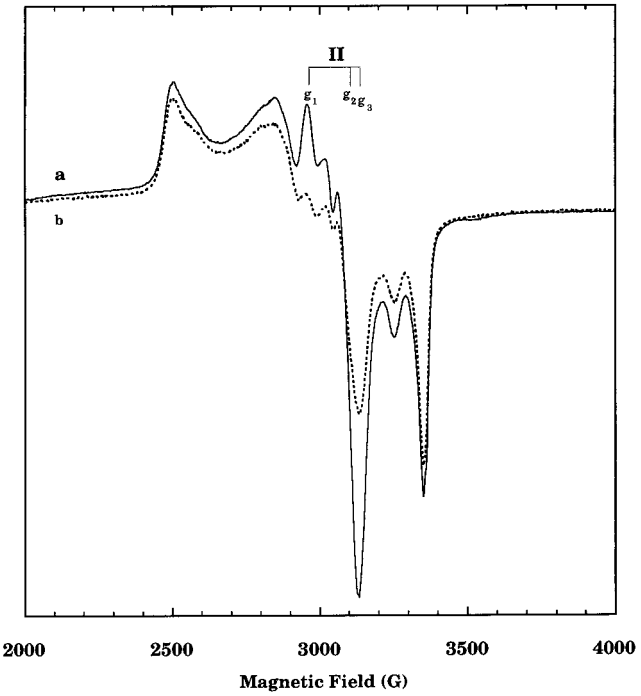


**Figure 4.** EPR spectrum (X band, 77 K) after 21 h UV-irradiation at 77 K under 300 Torr of hydrogen of (a) I-Nien-1.6 (solid line), (b) I-Nien-5 (dotted line).

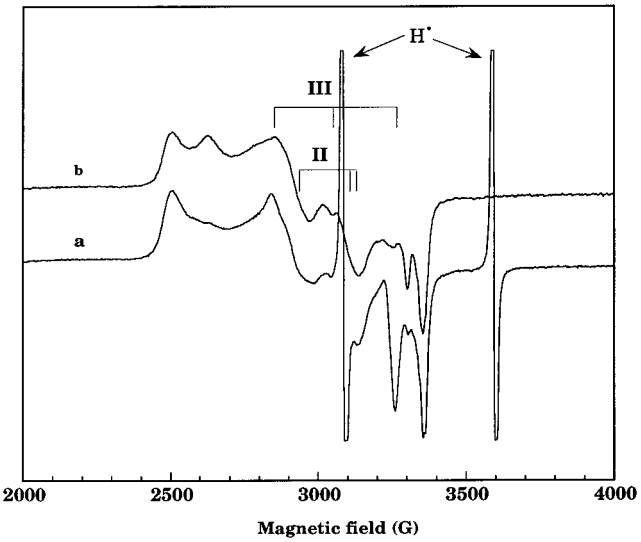


**Figure 5.** EPR spectrum (X band, 77 K) after 4 h UV-irradiation at 77 K under 300 Torr of hydrogen of E-$NiNH_3$ (a) without warming the sample before EPR spectrum recording, (b) after 30 min room-temperature warming of the sample before recording the EPR spectrum.

also shows that the shoulder at 2.270 may indeed be assigned to the $g_1$ of signal **II**. These results may be related to the above kinetic measurements by associating signal **I** to the reduction of precursor **1** and signal **II** to the reduction of precursor **2**. Signal **II** is more intense for E-Nien and I-Nien samples with low loading than for DPU or E-$NiNH_3$ samples (Figure 2). Other things being equal, the intensity of signal **II** decreases when the nickel content increases as illustrated in Figure 4 in the case of I-Nien.

Signal **III** is more intense when the photoreduction is carried out at 77 K and the EPR spectrum recorded at the same temperature without any intermediate warming of the sample (Figure 5). However, upon warming the irradiated sample to room temperature, signal **III** is partially transformed into signal **II**. Consequently, **III** is always weak for samples warmed to room temperature before EPR recording.

The relative intensities of the above EPR signals remain almost unchanged when the hydrogen pressure changes from 300 to 3 Torr. Only the overall intensity of the EPR spectra decreases with decreasing hydrogen pressure.

Upon outgassing at $10^{-5}$ Torr at room temperature, the above signals are reversibly removed and a broad axial signal **IV** ($g_{||} = 2.96$, $g_{\perp} = 2.090$) is observed. The above EPR signals are recovered upon subsequent hydrogen adsorption showing the reversibility of the phenomena described.

The EPR spectrum of the $Ni^{I}$ species obtained by thermal reduction at 250 °C under 300 Torr of hydrogen of E-$NiNH_3$ samples is shown on Figure 6. The same species described

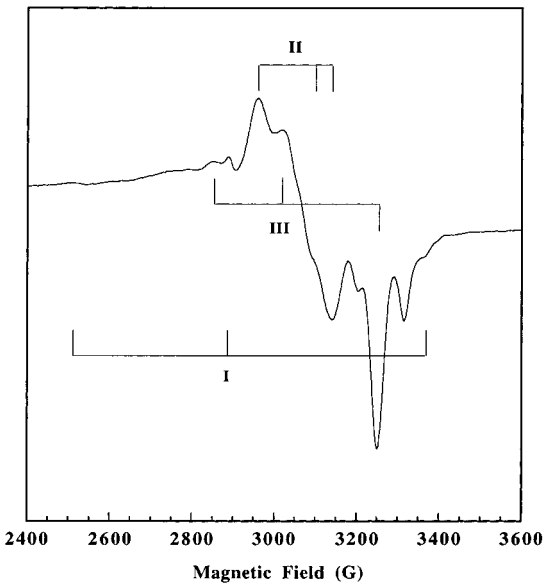


**Figure 6.** EPR spectrum (X band, 77 K) after 4 h thermal reduction at 250 °C under 300 Torr of hydrogen of E-$NiNH_3$.

above are visible but with different relative intensities. Signal **I** is very small, whereas signals **II** and **III** are predominant.

From the above findings, signal **I** on one hand and signals **II** and **III** on the other hand may be assigned to $Ni^{I}(H_2)_n$ complexes resulting from the reduction of two distinct $Ni^{II}$ precursors. They cannot be assigned to the same $Ni^{I}$ center coordinated to various numbers of hydrogen ligands as their relative intensities are independent of the hydrogen pressure. The $Ni^{II}$ precursor (**1**) yielding signal **I** is more sensitive to photoreduction, whereas the $Ni^{II}$ precursor (**2**) yielding signals **II** and **III** is selectively reduced by thermal reduction.

As we already mentioned, the unreduced samples contain isolated three-coordinated $Ni^{II}_{3c}$ cations and small NiO particles. The coordination number of $Ni^{II}$ ions located at the boundary of the NiO particules lies between 3 and 5 ($Ni^{II}_{xc}$ $3 \leqslant x \leqslant 5$). Indeed, one can assume that the original OH groups surrounding the $Ni^{II}$ ions located at the boundary of the NiO particles have been removed during the thermal treatment.

Signal **I** is expected to result from the reduction of isolated $Ni^{II}_{3c}$ (precursor **1**). UV-irradiation has already shown to be more efficient for the reduction of isolated $Cu^{II}$ into $Cu^{I}$ [18] and isolated $Mo^{VI}$ into $Mo^{V}$ [19] as compared to the corresponding oligomeric species.

Signals **II** and **III** are suggested to result from the reduction of three- or four-coordinated $Ni^{II}$ located at the boundary of NiO particules (precursor **2**). The wide UV-range of the lamp we used is expected to allow the electron transfer for the Ni−O bond in either isolated $Ni^{II}_{3c}$ or in other unsaturated $Ni^{II}$ precursors located at the boundary of the small NiO particles. However, in the same experimental conditions, low nickel loading E-Nien samples pretreated at 500 °C containing mainly isolated $Ni^{II}_{4c}$ [10,11] (as shown by diffuse reflectance spectroscopy in the UV−visible range and EXAFS) are very little photoreducible[20](i.e., the photoreduction degree measured by EPR or by the titration method based on CO chemisorption and described below is very low). This suggests that only three-coordinated $Ni^{II}$ precursors are photoreducible.

Signals **II** and **III** transform into **IV** upon evacuation at room temperature, whereas signal **I** was already reported to disappear in the same experimental conditions, probably because of a drastic decrease of the relaxation time in the resulting $Ni^{I}(O_3)$ species.[2]

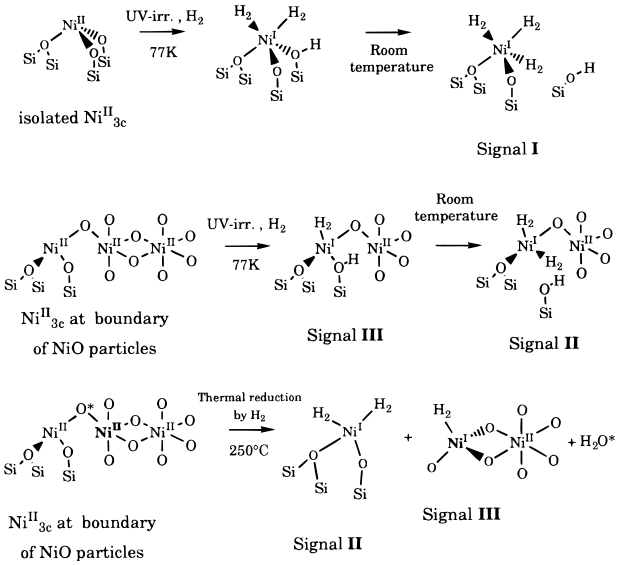


**Figure 7.** Possible mechanism for the formation of the various $Ni^{I}$ species during UV-photoreduction.

Table 1 summarizes the EPR parameters of $Ni^{I}$ species generated on various supports using UV-photoassisted reduction, and Table 2 describes the $Ni^{I}$ species reported after thermal reduction of various supported $Ni^{II}$ precursors. There is a variety of $Ni^{I}$ EPR signals, but most of them have **g** tensors different from the ones observed in this work. A possible assignment of the above EPR signals is given in Figure 7, which also summarizes the reactions occurring upon UV-irradiation at 77K and subsequent warming to room temperature.

Signal **I** may be considered as pseudoaxial with $g_1$, $g_2 \approx g_\perp > g_3 = g_{||} \approx g_e$, suggesting a $d_{z^2}$ ground state for the unpaired electron in agreement with a distorted tetrahedral or a trigonal-bipyramidal symmetry for the corresponding $Ni^{I}$ complex.[27] Signal **I** may be assigned either to the tetrahedral complex $(O)_2Ni^{I}(H_2)_2$ or to the bipyramidal $(O)_2Ni^{I}(H_2)_3$ species (where O stands for a silica surface oxygen atom) in agreement with the assignment of analogous EPR signals observed after thermal reduction of NiCaX samples[22] (Table 2). These complexes are suggested to result from the reduction of isolated $Ni^{II}_{3c}$ (Figure 7).

Signal **III** is pseudoaxial with $g_1$, $g_2 \approx g_\perp > g_3 = g_{||} \approx g_e$, suggesting a $d_{z^2}$ ground state for the unpaired electron again in agreement with a distorted tetrahedral or a trigonal-bipyramidal symmetry for the corresponding $Ni^{I}$ complex. It may be assigned to $(O)_2Ni^{I}(ONi^{II})(H_2)$ resulting from the photoreduction of three-coordinated $Ni^{II}$ located at the boundary of the small NiO particles thus coordinated via an oxygen bridge to a $Ni^{II}$ neighbor (Figure 7).

Signal **II** is pseudoaxial with $g_1 = g_{||} > g_2$, $g_3 \approx g_\perp > g_e$, suggesting a $d_{x^2-y^2}$ ground state for the single electron in agreement with an elongated tetrahedron or a distorted square-planar symmetry for the corresponding $Ni^{I}$ complex. **II** may therefore be assigned to the distorted square-planar $(O)(ONi^{II})$-$Ni^{I}(H_2)_2$ resulting from the transformation at room temperature of the $Ni^{I}$ species associated to signal **III** (Figure 7).

Signal **IV** is assigned to the $(O)_2Ni^{I}(ONi^{II}_{xc})$ ($x = 5$) complex. The symmetry constrains derived from the connection of this site to a NiO particle do not yield the same drastic decrease of relaxation time responsible for the disappearance of the EPR signal of isolated $Ni^{II}_{3c}$.

The number of dihydrogen ligands bound to $Ni^{I}$ cannot be easily determined because of the absence of any superhyperfine

**TABLE 1: EPR Parameters of $Ni^{I}$ Species Generated by UV-Irradiation in the Presence of $H_2$ of Nickel Deposited on Various Supports**

| sample | treatment | orthorhombic $Ni^{I}$ | axial $Ni^{I}$ | ref |
|---|---|---|---|---|
| $Ni/Al_2O_3$ | UV-reduction in $H_2$ | $g_1 = 2.540$<br>$g_2 = 2.280$<br>$g_3 = 2.035$ | $g_{\|\|} = 2.440$<br>$g_\perp = 2.072$ | 9 |
| $Ni/Al_2O_3$ | UV-reduction in $H_2$ | $g_1 = 2.499$<br>$g_2 = 2.325$<br>$g_3 = 2.068$ | $g_{\|\|} = 2.337$<br>$g_\perp = 2.075$ | 9 |
| $Ni/SiO_2$ | | $g_1 = 2.640$<br>$g_2 = 2.300$<br>$g_3 = 2.015$<br>$Ni^{I}(H_2)$ distorted tetrahedron | | 21 |
| $Ni/SiO_2$ | UV-reduction in $H_2$ | **I**<br>$g_1 = 2.680$<br>$g_2 = 2.320$<br>$g_3 = 2.003$<br>**II**<br>$g_1 = 2.270$<br>$g_2 = 2.171$<br>$g_3 = 2.144$<br>**III**<br>$g_1 = 2.366$<br>$g_2 = 2.215$<br>$g_3 = 2.062$ | **IV**<br>$g_{\|\|} = 2.96$<br>$g_\perp = 2.090$ | this work |

**TABLE 2: EPR Parameters of $Ni^{I}$ Species Generated by Thermal Reduction of Nickel Deposited on Various Supports**

| sample | treatment | orthorhombic $Ni^{I}$ | axial $Ni^{I}$ | ref |
|---|---|---|---|---|
| Ni−LaX | thermal reduction in $H_2$ | | $g_{\|\|} = 2.68$<br>$g_\perp = 2.096$<br>$Ni^{I}(O)_3(H_2)$ in $S_{II}$ or $S_{II'}$ | 8 |
| NiCa−X | thermal reduction in $H_2$ | $g_1 = 2.502$<br>$g_2 = 2.291$<br>$g_3 = 2.012$<br>$Ni^{I}(O)_2(H_2)_2$ or $Ni^{I}(O)_2(H_2)_3$ in the supercage | | 22 |
| NiCa−X | thermal reduction in $H_2$ | | $g_{\|\|} = 2.69$<br>$g_\perp = 2.096$ | 23 |
| $Ni/SiO_2$ | thermal reduction in $H_2$ | | $g_{\|\|} = 2.75$<br>$g_\perp = 2.097$ | 24 |
| NiH−SAPO-11 | thermal evacuation | $g_1 = 2.165$<br>$g_2 = 2.096$<br>$g_3 = 2.062$<br>$Ni^{I}(O)_3(OH)_n$ near $S_{II}$ | $g_{\|\|} = 2.461$<br>$g_\perp = 2.098$<br>$Ni^{I}(O)_3$ in $S_{II}$ and $Ni^{I}(O)_6$ in $S_I$ | 25 |
| NiH−SAPO-5 | thermal evacuation | | $g_{\|\|} = 2.479$<br>$g_\perp = 2.111$<br>$Ni^{I}(O)_3$ | 26 |
| | thermal reduction in $H_2$ | | $g_{\|\|} = 2.335$<br>$g_\perp = 2.071$<br>$Ni^{I}(H_2)_n$<br>$g_{\|\|} = 2.479$<br>$g_\perp = 2.111$<br>$Ni^{I}(O)_6$ | |

structure on the EPR spectra. Isolated $Ni^{II}{}_{3c}$ precursors are expected to yield $Ni^{I}$ complexes with up to four hydrogen ligands because $Ni^{I}$ likes to be in 5-fold coordination and ligands from the gas phase have been shown to be able to substitute the surface oxygen atom ligands.[28] EPR signal **I** is therefore assigned to the bipyramidal $(O)_2Ni^{I}(H_2)_3$ (Figure 7). However, the number of hydrogen ligands that may be bound to the nonisolated sites is expected to be smaller because of steric constraints. The square-planar $(O)_2Ni^{I}(H_2)_2$ has been therefore assigned to signal **II** resulting from the reduction of boundary $Ni^{II}{}_{3c}$ sites (**2**) (Figure 7).

It is not obvious to include the above $Ni^{I}(H_2)$ complexes in one of the dihydrogen complex classes[4] mentioned in the Introduction. Indeed, we can only rely on the EPR signals that exhibit no superhyperfine structure, in order to propose a molecular structure. It is not possible to obtain nuclear magnetic resonance data concerning these paramagnetic complexes nor X-ray diffraction data because they are grafted onto amorphous silica; consequently, we do not have access to the H−H bond length. However, as these complexes are not very stable; (i) they decompose by evacuation at room temperature and (ii) $H_2$ is easily substituted by any other ligand, even $N_2$, and because the properties of dihydrogen are not obviously modified upon coordination, our $Ni^{I}$−dihydrogen complexes may be included in the unstretched Kubas-like type.

The analysis of the reduced nickel EPR signals suggests the presence of two types of $Ni^{II}{}_{3c}$ precursors that could not be distinguished by EXAFS and DRS studies. Low-temperature FTIR studies using CO as a probe performed on unreduced E-Nien or E-$NiNH_3$ samples of low nickel loading show the formation of two $Ni^{II}(CO)_2$ complexes[29] and therefore also suggest the presence of two $Ni^{II}{}_{3c}$ precursors in the unreduced samples. One of these complexes has two equivalent CO ligands that may be bound to isolated precursor $Ni^{II}{}_{3c}$ **1**, whereas the other complex has two inequivalent CO ligands that may be bound to precursor **2**. The connection of precursor **2** to the NiO particle may be responsible for the distortion of the resulting $Ni^{II}(CO)_2$ complex.

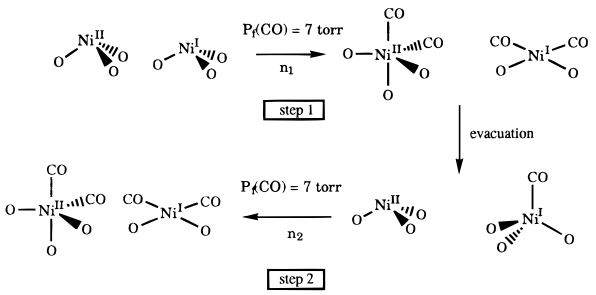


**Figure 8.** Principles of the titration of $Ni^I$ using CO adsorption measurements.

**Titration of $Ni^I$ Ions by CO Adsorption Measurements.** After evacuation of hydrogen, the partially photoreduced samples contain a mixture of supported $Ni^I$ ($n_{Ni^I}$) and unreduced $Ni^{II}$ ($n_{Ni^{II}}$) cations. The spectroscopic studies support the absence of both metallic nickel particles or clusters. On the infrared (IR) spectra obtained using CO as a probe, there is no absorption band in the range expected for the streching vibration of CO interacting with either isolated $Ni^0$ or metallic particles.[30] There is no ferromagnetic resonance of the samples, indicating the absence of nickel particles of size larger than 10 Å in diameter. Finally, the green color of the reduced samples is not correlated with absorption bands reported by Schoonheydt et al.[8,31] at 740 and 364 nm or at 294 and 263 nm for $Ni^0$ clusters of molecular size or larger ones, respectively. After photoreduction, only one DRS band is observed at 838 nm, which was attributed to $Ni^I{}_{4c}$.[2] CO adsorption measurements performed at low CO pressure may therefore allow us to evaluate the amount of both $Ni^I$ and $Ni^{II}$ centers accessible to carbon monoxide.

The various $Ni^I(CO)_n$ ($n$ =1−4) complexes formed upon adsorption of suitable pressures of CO on the photoreduced samples have been previously characterized by EPR[28] or IR spectroscopy[30] in the case of E-$NiNH_3$ samples. For the other classes of samples, it was checked that the $Ni^I$−carbonyl complexes had the same stability domains. The only difference concerns $(O)_3Ni^I(CO)$ that could be obtained by evacuation at room temperature overnight instead of by evacuation at 60 °C for 15 min in the case of E-$NiNH_3$.

The measurements are carried out in two steps. A first isothermal CO adsorption (step 1) is performed so that the final CO pressure is about 7 Torr. In these conditions, $n_1$ molecules of CO are adsorbed. The three-coordinated $Ni^I$ ions are selectively transformed into the square-planar $(O)_2Ni^I(CO)_2$ complex whereas $Ni^{II}$ is expected to coordinate one or two CO ligands[28,30] (Figure 8). The number of CO molecules attached to $Ni^{II}$ is not known and is referred to as α. A subsequent suitable evacuation regenerates the starting $Ni^{II}$ species together with the monocarbonyl $Ni^I$ complex. A second CO chemisorption ($n_2$ molecules of CO, step 2) in the same experimental conditions as in step 1 (final CO pressure of 7 Torr) yields again the $Ni^I$−dicarbonyl and $Ni^{II}$−α-carbonyl complexes (Figure 8).

The following equations result:

$$n_1 = 2n_{NiI} + \alpha n_{NiII} \quad (1)$$

$$n_2 = n_{NiI} + \alpha n_{NiII} \quad (2)$$

The amount of $Ni^I$ may therefore be calculated by subtracting eq 2 from eq 1 as follows:

$$n_{NiI} = n_1 - n_2$$

Table 3 summarizes the results of titration obtained for the four types of samples. The following reduction degree order results:

E-$NiNH_3$ (20%) < DPU (24%) < I-Nien (35%) < E-Nien (40%)

**TABLE 3: Titration of $Ni^I$ in the Various Classes of Photoreduced Samples. Comparaison of CO Adsorption and EPR Measurements**

| sample | nickel loading (wt %) | reduction time (h) | reduction degree (%) | |
|---|---|---|---|---|
| | | | CO adsorption | EPR |
| E-Nien | 1.5 | 1 | 17 | - |
| E-Nien | 1.5 | 11 | 42 | 42 |
| I-Nien | 1.6 | 19 | 35 | 37 |
| E-$NiNH_3$ | 1.4 | 20 | 18 | 18 |
| DPU | 2.8 | 30 | 24 | 24 |

**Comparison with EPR.** For each class of samples, the amount of $Ni^I$ species was evaluated by double integration of the EPR signals obtained after at least 17 h of photoreduction under 300 Torr of hydrogen. The EPR spectra of the various samples were recorded in the same EPR tube in order to compare their relative intensities. The reduction degree of E-Nien was assumed to be 42% as measured by CO adsorption. The relative reduction degrees obtained for the other samples are listed in Table 3. The CO adsorption measurements appear to be in good agreement with the relative reduction degrees estimated by EPR.

**New Titration Method.** When several surface species are present, it appears attractive to be able to identify and to quantify their concentrations. This work has evidenced the presence of at least two types of $Ni^{II}$ precursors and two oxidation states of nickel.

Because there is no suitable EPR standard[6,7] to quantitatively determine the absolute concentration of $Ni^I$ ions, the measurements can only be made within about 20%. A new $Ni^I$ titration method was therefore proposed in this work. Two CO chemisorption steps allow elimination of the contribution of unreduced $Ni^{II}$ to CO adsorption. The reduction degree is then obtained with a relative error only related to the precision of the pressure measurements, i.e., about 3%. The CO chemisorption measurements are in agreement with relative estimations of the $Ni^I$ content of the photoreduced samples based on EPR (Table 3). The titration method is therefore validated.

The reduction degree is assumed to be proportional to the amount of isolated $Ni^{II}{}_{3c}$ present in the unreduced sample.[2] The following increasing order of $Ni^{II}{}_{3c}$ concentration in the unreduced but thermally treated samples may therefore be derived:

$$\text{E-NiNH}_3 \approx \text{DPU} < \text{I-Nien} < \text{E-Nien}$$

EXAFS measurements were not able to quantify the relative amount of isolated $Ni^{II}{}_{3c}$ species in the above samples. Moreover EXAFS was not able to detect the NiO phase in E-Nien samples,[10,11] suggesting that the concentration of this phase is lower than 10%, which is the lower limit of EXAFS detection. The titration of $Ni^I$ results therefore in a better understanding of the unreduced samples.

The partial reduction of the samples may be explained by a photoreduction carried out at too low temperature. Indeed an optimum photoreduction temperature of 95 °C was reported for silica−alumina supported nickel samples.[32]

## Conclusions

Whatever the deposition method of nickel onto silica, the reduction by UV-irradiation of the samples yields three silica supported $Ni^I(H_2)_n$ complexes (EPR signals **I**, **II**, and **III**). EPR

signal **IV** is observed upon evacuation of hydrogen at room temperature. The relative proportions of the $Ni^{I}(H_2)_n$ complexes depend on the nickel deposition method and on the nickel loading of the samples because they result from the reduction of either isolated three-coordinated $Ni^{II}$ ions or of three-coordinated $Ni^{II}$ precursors located at the boundary of small NiO particles.

The total amount of $Ni^{I}$ was measured using a new titration method based on CO chemisorption. The highest reduction degree ($[Ni^{I}/Ni_{total}] = 40\%$) is obtained for samples where $Ni^{2+}$ was introduced by cationic exchange of the silica support with $[Ni(en)_3]^{2+}$. The results are consistent with concomitant electron paramagnetic resonance measurements.

The $Ni^{I}$ reduction degree is assumed to be proportional to the amount of the starting isolated $Ni^{II}_{3c}$ precursors. The above EPR studies and $Ni^{I}$ titration allow therefore to precise the EXAFS results by the proposal of the following increasing order of $Ni^{II}_{3c}$ amount for the unreduced but thermally treated samples:

$$E\text{-}NiNH_3 \approx DPU < I\text{-}Nien < E\text{-}Nien$$

**Acknowledgment.** The authors thank L. Bonneviot and B. Shelimov for very fruitful discussions.

## References and Notes

(1) Lepetit, C.; Kermarec, M.; Olivier, D. *J. Mol. Catal.* **1989**, *51*, 93.
(2) Bonneviot, L.; Cai, F. X.; Che, M.; Kermarec, M.; Legendre, O.; Lepetit, C.; Olivier, D. *J. Phys. Chem.* **1987**, *91*, 5912.
(3) Crabtree, R. H. *Angew. Chem., Int. Ed. Engl.* **1993**, *32*, 789.
(4) Chaudret, B. Actual. Chim. **1996**, *7*, 26.
(5) Kubas, G. J. *Acc. Chem. Res.* **1988**, *21*, 120.
(6) Dyrek, K.; Madej, A.; Mazur, E.; Rokosz, A.; Rusiecka, M. *Wiss. Z. Friedrich-Schiller-Univ. Jena, Naturwiss. Reihe* **1988**, *37*, 781.
(7) Dyrek, K.; Rokosz, A.; Madej, A. *Appl. Magn. Reson.* **1994**, *6*, 309.
(8) Schoonheydt, R. A.; Vaesen, I.; Leeman, H. *J. Phys. Chem.* **1989**, *93*, 1515.
(9) Bonneviot, L.; Che, M.; Dyrek, K.; Schöllner, R.; Wendt, G. *J. Phys. Chem.* **1986**, *90*, 2379.
(10) Carriat, J. Y. Thesis Université Pierre et Marie Curie, 1994.
(11) Carriat, J. Y.; Che, M.; Kermarec, M.; Verdaguer, M.; Michalowicz, A. *J. Am. Chem. Soc.* **1998**, *120*, 2059.
(12) Clause, O.; Kermarec, M.; Bonneviot, L.; Villain, F.; Che, M. *J. Am. Chem. Soc.* **1992**, *114*, 4709.
(13) Cheng, Z. X.; Louis, C.; Che, M. *Stud. Surf. Sci. Catal.* **1995**, *91*, 1027.
(14) Bonneviot, L.; Clause, O.; Che, M.; Manceau, A.; Dexpert, H. *Catal. Today* **1989**, *6*, 39.
(15) Lepetit, C.; Kermarec, M.; Olivier, D. *J. Mol. Catal.* **1989**, *51*, 73.
(16) Clause, O.; Bonneviot, L.; Che, M.; Dexpert, H. *J. Catal.* **1991**, *130*, 21.
(17) Klimchuck, E. G.; Shelimov, B. N.; Kazanskii, V. B. *Kinet. Katal.* **1985**, *26*, 396.
(18) Amara, M.; Bettahar, M.; Gengembre, L.; Olivier, D. *Appl. Catal.* **1987**, *35*, 153.
(19) Shelimov, B. N.; Pershin, A. N.; Kazansky, V. B. *J. Catal.* **1980**, *64*, 426.
(20) Martinez-Arias, A.; Lepetit, C. To be published.
(21) Kazansky, V. B.; Elev, I. V.; Shelimov, B. N. *J. Mol. Catal.* **1983**, *21*, 265.
(22) Michalik, J.; Narayana, M.; Kevan, L. *J. Phys. Chem.* **1984**, *88*, 5236.
(23) Olivier, D.; Richard, M.; Che, M.; Bozon-Verduraz, F.; Clarkson, R. B. *J. Phys. Chem.* **1980**, *84*, 420.
(24) Bonneviot, L.; Olivier, D.; Che, M. *J. Chem. Soc., Chem. Commun.* **1982**, 952.
(25) Azuma, N.; Kevan, L. *J. Phys. Chem.* **1995**, *99*, 5083.
(26) Azuma, N.; Hartmann, M.; Kevan, L. *J. Phys. Chem.* **1995**, *99*, 6670.
(27) Hathaway, B. J.; Billing, D. E. *Coord. Chem. Rev.* **1970**, *5*, 143.
(28) Bonneviot, L.; Olivier, D.; Che, M. *J. Mol. Catal.* **1983**, *21*, 415.
(29) Kermarec, M. et al. To be published.
(30) Kermarec, M.; Delafosse, D.; Che, M. *J. Chem. Soc., Chem. Commun.* **1983**, 411.
(31) Schoonheydt, R. A.; Roodhooft, D. J. *J. Phys. Chem.* **1986**, *90*, 6319.
(32) Spinici, R.; Tofanari, A. *Mater. Chem. Phys.* **1990**, *25*, 375.